Concrete pavement slab under blast loads

Bibiana María Luccioni[a],*, Mariela Luege[b]

[a]*Structures Institute, National University of Tucumán, CONICET, Juan B. Terán 375, 4107 Yerba Buena, Tucumán, Argentina*
[b]*Structures Institute, National University of Tucumán, CONICET, Av. Roca 1800, 4000 S.M. de Tucumán, Argentina*

Abstract

The main objective of this paper is the analysis of the behaviour of concrete pavements subjected to blast loads produced by the detonation of high explosive charges above them. This subject is of particular interest in terrorist attacks in cities, since important conclusions about the location and magnitude of the explosive charge can be drawn from simple observation of the pavement damage. Experimental results for a concrete slab lying on the ground and subjected to blast loads are presented. The slab was lying on the ground and was tested with different amounts of explosive suspended in air over it. Numerical results are compared with those obtained with a simplified plastic limit analysis and those obtained with two types of numerical simulations performed with two different codes. Some conclusions about the effect of the blast load on the concrete slab and about different tools available for the analysis of this type of problem are stated in the paper.
© 2004 Elsevier Ltd. All rights reserved.

Keywords: Concrete slabs; Blast load; Experimental analysis; Limit analysis; Numerical analysis

1. Introduction

Due to different accidental or intentional events in connection with important structures all over the world, blast loads have received considerable attention in recent years [1–3]. The activity related to terrorist attacks has increased and, unfortunately, the present tendency suggests that it will be even larger in the future. This paper is concerned with the effect of dynamic loading

---

*Corresponding author. Tel.: +54 381 4364087; fax: +54 381 4364087.
  E-mail address: bluccioni@herrera.unt.edu.ar (B.M. Luccioni).

produced by the detonation of high explosives on concrete pavements, a situation likely in a significant number of terrorist attacks.

When the attack has already occurred, a very important issue is the determination of the location of the explosion and the mass of explosive used. A useful tool to achieve this objective is the evidence of the crater generated by the explosion in the pavement.

A blast wave originating from a closed or free explosive detonation behaves, when interacting with structures, as a short duration dynamic load. In recent years, studies have shown that such loads with short duration and high magnitude influence significantly the response of the structure and can modify substantially the expected material behaviour [4–9].

Much research has been carried out in recent years concerning the behaviour of structural elements and materials under blast loads. Experimental results about the behaviour of steel [10,11], concrete [12,13] and fibre reinforced [14] panels subjected to blast loads can be found in References.

In the literature, beams, slabs and shells under blast loads are mostly studied with limit analysis theory which assumes a rigid-plastic behaviour for the material [12,15]. Yi [12] tested concrete slabs under blast loads and studied the behaviour using a non-linear dynamic analysis. For close-in explosions the problem was solved by an approximate procedure. First a check is performed to determine if the zone just below the load has disintegrated or not. If it has disintegrated, the level of damage is estimated. The tension failure of the other side of the plate is also studied with the aid of elastic theory. For the assessment of the dynamic displacement of the plate centre, a one degree of freedom model is used.

On the other hand, with the rapid development of computer hardware over the last decades, it has become possible to make detailed numerical simulations of blast loads on personal computers, significantly increasing the availability of these methods.

Although there are still many uncertainties, material behaviour under blast loads has been widely studied experimentally [16–19] and many sophisticated numerical models have been proposed, especially for steel and concrete [4,6,9,20–23]. The behaviour of concrete under blast loads is characterized by a different response in tension and compression, the progressive degradation of elastic properties accompanied by increasing permanent strains and the dependence of the strength, stiffness and fracture energy on strain rate. This last feature has been normally taken into account through viscoplastic models or rate-dependent damage models. [4–9]. These models have been included in different computer programs [4,23,24], which can be used for the analysis of the blast behaviour of structural elements and small structures and validated with available experimental results.

In this work the experimental results for a concrete plate lying on the ground, subjected to different blast loads, are compared with the results of a simplified limit analysis and numerical results obtained with the ABAQUS/Explicit [25] program and AUTODYN 2D and 3D [26]. The dimensions of the damage zone are also compared with those obtained by Yi [12] and with the dimensions of the craters that would have been produced by the explosions acting directly on the ground.

2. Experimental tests

The experimental results described below belong to a series of tests carried out by the Structures Institute of the National University of Tucumán. The complete series of tests consisted of the

detonation of explosive charges lying on the ground and elevated above the ground [10,11] and above a concrete plate lying on the ground. Pressure loads were registered at different distances, together with the size of the craters formed in the soil, the response of two metallic panels and the cracking and damage patterns of the concrete slab. In order to measure the overpressure generated by shock waves, pressure sensors were used. In addition, accelerometers were used to measure the dynamic response of the steel plates. A dynamic strain amplifier amplified the signal generated by the accelerometers. A data acquisition board was mounted on a notebook computer in order to record and process the signals by means of data acquisition software.

This paper is focused on the behaviour of the concrete slab. The geometrical configuration of the reinforced concrete slab lying on the ground is shown in Fig. 1. The reinforcement consisted of 4.2 mm diameter bars spaced 150 mm in both directions. The average compressive strength of the concrete (25 MPa) was obtained from compression tests at 28 days of a series of cylindical proof samples cast with the same concrete as the slab.

The soil was soft-OL type (Unified System for the Classification of Soils), i.e. an organic soil without fine particles (more than 50% passing through sieve #200) with a liquid limit of less than 50 and a plastic limit of less than 4.

The load location on the concrete slab is also depicted in Fig. 1. Spherical explosive charges of 5 and 12.5 kg of Gelamon VF80 were employed placed at 0.50 m height above the top surface of the slab as shown in Fig. 2. The nominal TNT equivalence factor for Gelamon VF80 is 0.8. Table 1 summarizes the sequence of the applied loads and their locations.

The cracking patterns registered after the experimental tests are shown in Figs. 3 and 4. The charge of 5 kg Gelamón produced the crushing of concrete in a circular zone of about 250 mm diameter, while the diameter of the concrete crushing zone was about 300 mm for the 12.5 kg charge. The first test produced a fracture of the slab parallel to the short side. As a result, for the following detonations, the original slab behaved as two square independent slabs. Furthermore, circumferential cracks could be found around the crushing zone in both cases. Such cracks defined two circumferences, the first one with a diameter of about 1.0 m and the second one coincident
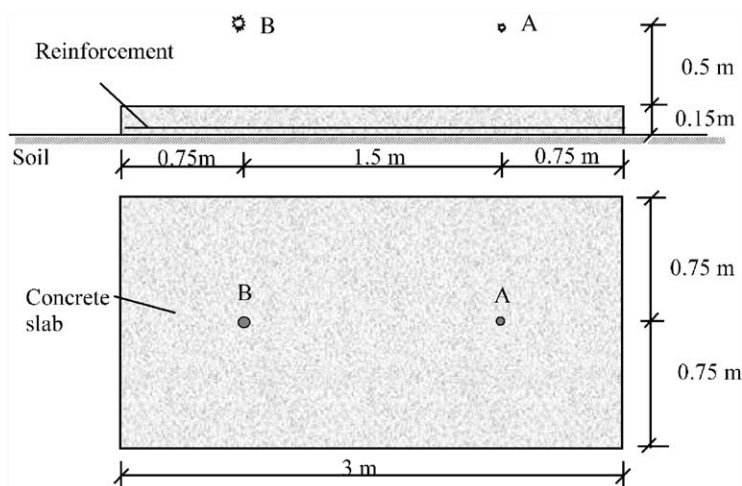

Fig. 1. Concrete slab dimensions and charge positions.

Fig. 2. Placement of the explosive charge suspended above the slab.

Table 1
Explosion sequence

Test	Position	Height (m)	Charge (kg of Gelamón)
1	A	0.5	5
2	A	0.5	5
3	B	0.5	12.5

with the border of the slab and both centred on the point on the slab directly beneath the charge. Radial cracks could be seen quite clearly, in particular the ones parallel to the sides of the slab.

The relative maximum vertical displacements were found to be located directly beneath the two charge locations A and B. The values registered were 23 mm for position A, and 75 mm for position B.

The relative diameter of the crushing zone D to the height of the charge h is shown in Fig. 5a as a function of the inverse of the scaled distance $W^{1/3}/h$. The results obtained by Yu [12] for explosions in direct contact with a concrete plate have also been included in Fig. 5a together with the results corresponding to craters in soils [27]. It can be observed that, although the crushing
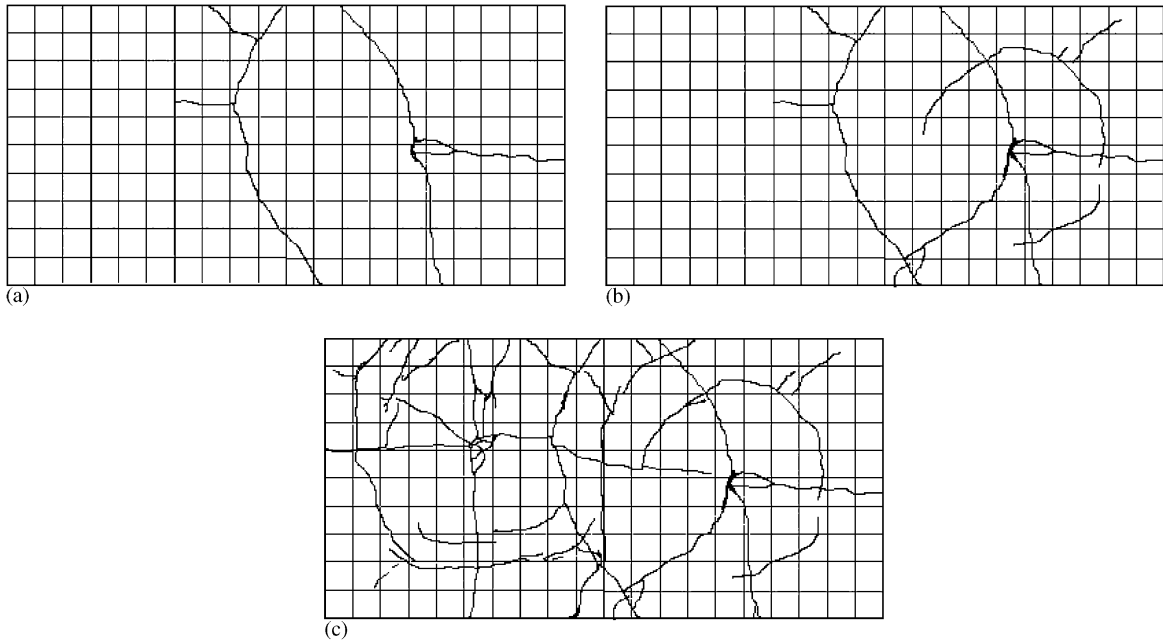
Fig. 3. Cracking patterns (a) after test 1, (b) after test 2, (c) after test 3.

zone in concrete is always smaller than the corresponding crater in soil, the results follow the same trend. Fig. 5b shows the results of craters on concrete slabs and a curve corresponding to and exponential approximation of the relation presented in Eq. (1). This equation can be used either for the estimation of explosive charges from crater diameters or crater dimensions from explosive charge, depending on what the purpose of the analysis is

$$\ln(3.63 D/h) = 0.1838(W^{1/3}/h). \tag{1}$$

3. Limit analysis

The limit analysis of plates with different geometry and boundary conditions subjected to dynamic loads is well documented in the literature [15].

The equation of motion of a circular rigid perfectly plastic plate, of radius a, simply supported on its boundary and subjected to uniform distributed pressure, as indicated in Fig. 6a, is given by Lubliner [15]

$$\frac{\partial(rM_r)}{\partial r} - M_\theta = \int_0^r \left(p + \mu \frac{\partial^2 w}{\partial t^2} \right) r \, dr, \tag{2}$$

where μ is mass per unit area, p is pressure, M_r is radial moment, M_θ is circumferential moment, w is vertical displacement and r is radius. The generalized Tresca yield criterion with ultimate bending moment M_u is assumed (see Fig. 6b). All the plate is supposed to be in regime BC
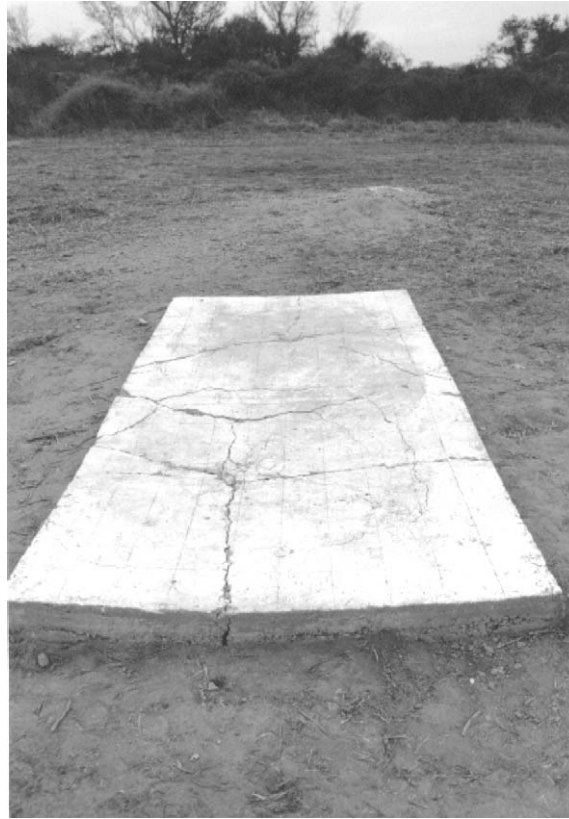
Fig. 4. Damage of the slab after the tests.

(Fig. 6b): $M_\theta = M_u$, whereas for the centre of the plate $M_r = M_\theta = M_u$ (Point C in Fig. 6b). Consequently, it can be assumed that the plate has a conic deformation (Fig. 6c) described by the following equation:

$$w(r, t) = -\Delta(t)\left[1 - \frac{r}{a}\right],\tag{3}$$

where the parameter $\Delta(t)$ represents the deflection of plate centre at time t.

Eq. (3) together with Eq. (2), $M_\theta = M_u$ and the boundary condition $M_r(a, t) = 0$, gives,

$$M_r = M_U - \frac{r^2}{6}\left[p - (p - p_U)\left(2 - \frac{r}{a}\right)\right],\tag{4}$$

where $p_U = 6M_U/a^2$ is the static limit pressure.

Eq. (4) is valid for $p \leqslant 2p_U$. For the case $p > 2p_U$, the plate configuration is a truncated cone, with a circular hinge of radius r_0 separating the external conic zone from the internal one, see Fig. 6d. The latter corresponds to the point B of the Tresca criterion ($M_r = M_\theta = M_U$) and the equations of motion that result are

$$\mu\frac{\partial^2\Delta}{\partial t^2} = p \quad \text{for } r \leqslant r_0,\tag{5a}$$
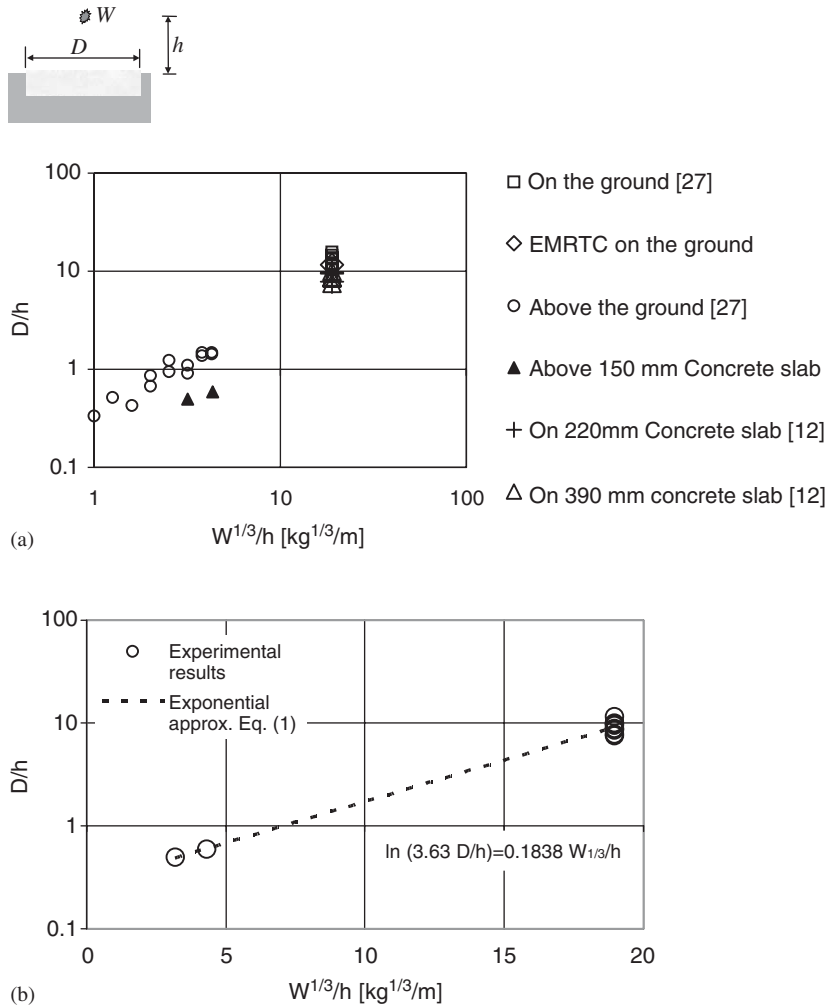
Fig. 5. Variation of the relative diameter of the crushing zone D/h as a function of the inverse of the scaled distance $W^{1/3}/h$ (a) comparison with the dimensions of craters in soils, (b) exponential approximation.

$$\frac{\partial(rM_{\mathrm{r}})}{\partial r} = M_U - \frac{p(2r^3 - 3r_0 r^2 + r_0^3)}{6(a - r_0)} \quad \text{for } r > r_0. \tag{5b}$$

Integrating Eq. (5b) with the initial condition $M_{\mathrm{r}} = M_U$ at $r = r_0$, the following cubic equation is obtained for r_0:

$$\left(1 - \frac{r_0}{a}\right)^2 \left(1 + \frac{r_0}{a}\right) = \frac{2p_U}{p}. \tag{6}$$

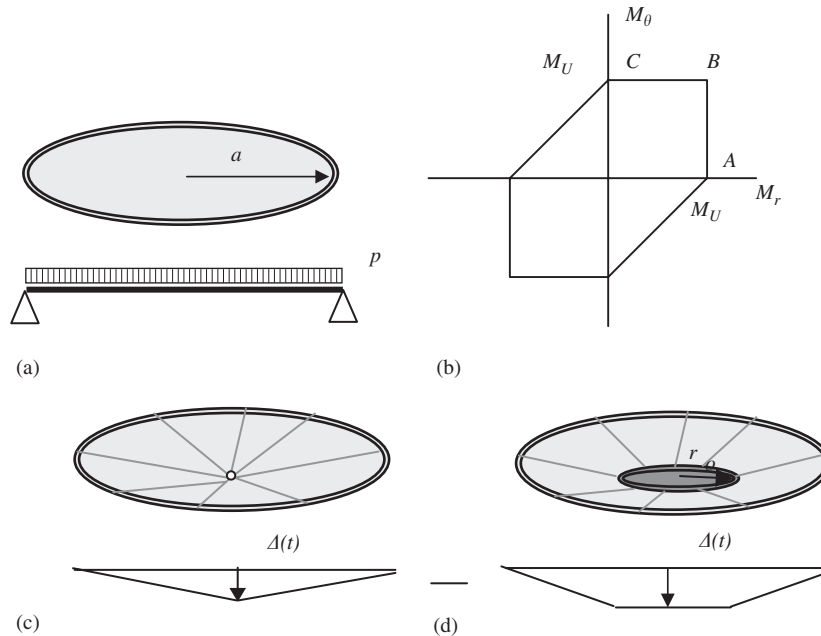Notice that the substitution of $r_0 = 0$ in Eq. (6) gives $p = 2\,p_U$.

Fig. 6. Circular rigid perfectly plastic plate (a) Undeformed shape, (b) Tresca Criterion, (c) Ultimate configuration for $p \leqslant 2\,p_{\mathrm{u}}$ and (d) Ultimate configuration for $p > 2\,p_{\mathrm{u}}$.

According to Lubliner [15], an estimation of the upper bound for the limit load of a clamped plate of arbitrary shape can be obtained from the previous results. It could be considered that the largest circle that can fit into the plate is a hinge. The material inside this circle collapses like a clamped circular plate and the material outside it remains rigid.

An approximate solution for the tested slab can be obtained carrying out ultimate analysis, making the assumption that the soil under the slab does not alter its collapse mechanism. Following Lubliner [15], a circular clamped plate of radius $a = 0.75\,\mathrm{m}$ is considered. As the reinforcement is placed at the back face of the plate, the negative ultimate moment is almost zero and the circular plate can be supposed to be simply supported at its border. Therefore, Eq. (6) can be used to estimate an upper limit for the ultimate load or an upper limit to r_0. The ultimate positive moment is defined by the yielding of the reinforcement. The external cone radius r_0, can be obtained from Eq. (6), with $p_U = 6M_U/a^2 = 9.28\,\mathrm{MPa}$. The results obtained can be summarized as follows:

- Position A: 4 kg TNT at 0.5 m height ($p = 63.8\,\mathrm{MPa}$): $r_0 = 0.45\,\mathrm{m}$,
- Position B: 10 kg TNT at 0.5 m height ($p = 151.1\,\mathrm{MPa}$): $r_0 = 0.55\,\mathrm{m}$.

It can be observed that the radius r_0, calculated using the classical theory, is almost coincident with the radius of the smallest circumferences that are shown in Fig. 3. It can be assumed that the slab responded as a simply supported circular plate whose boundary was the external circumferential crack, almost coincident to the border of the slab. As the slab was slightly

reinforced, the reinforcing steel was not enough to spread the cracking effect, like in the continuum model used, and appreciable discrete cracks were formed. Moreover, as the external crack was not exactly circular but parallel to the sides of the slabs radial cracks can be found where $M_\theta = M_U$ and where the plastic deformation was concentrated.

4. Numerical simulation

The numerical analysis has been carried out with two different codes: the finite element program ABAQUS/Explicit 5.8-18 [25] and the hydrocode AUTODYN v. 4.3 [26].

4.1. Finite element program [25]

The finite element mesh of the whole system is given in Fig. 7. The slab was modelled with 1000 C3D8R tri-dimensional elements arranged in five layers of equal height. The reinforcement was modelled by adding two layers of steel (REBAR) placed between the first and second layer and in both directions 1 and 2.

For the soil, a combination of C3D8R tri-dimensional elements and CIN3D8 semi-infinite tri-dimensional elements were used, so that the soil could be approximately modelled as a semi-infinite space. The semi-infinite elements represent smooth boundaries through which energy can pass without being absorbed or reflected.

Materials were characterized using simple constitutive models, with the idea of capturing the global response of the system with the use of few observable parameters.
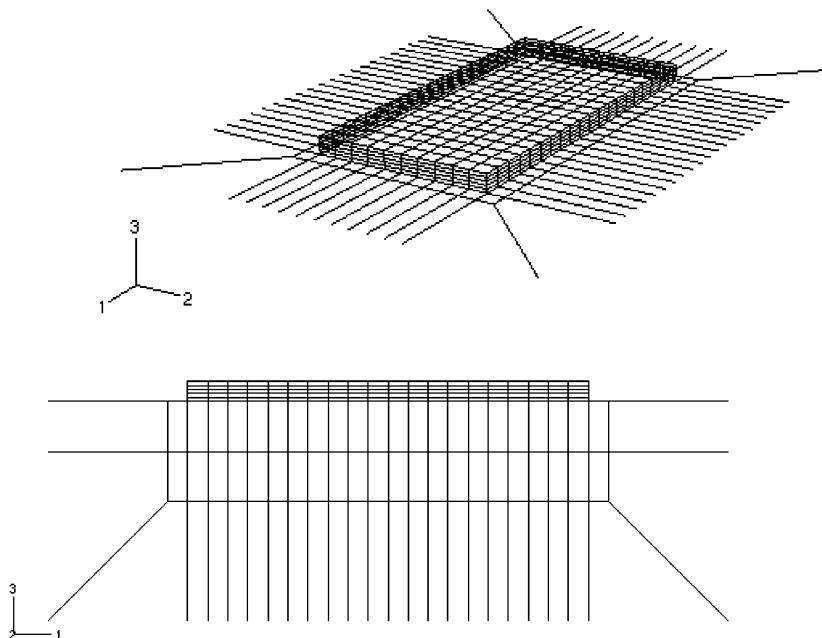

Fig. 7. Finite element mesh (ABAQUS CAE 2-5).

An elasto-plastic material model with properties dependent on the strain rate has been used for the concrete. The material model is the extended Drucker–Prager with the parameters reported in Table 2.

Steel was characterized with an elasto-perfectly plastic model with the properties presented in Table 3.

The elasto-plastic material model used for the soil was the modified Drucker–Prager/Cap. All the model material properties were estimated on the basis of the type of soil (due to the lack of experimental data) and are presented in Table 4.

The detonation of an explosive charge generates a pressure wave in the air. The evolution of the pressure is characterized by a strong increment of pressure at the wave front followed by an exponential fall. The peak value of the overpressure depends on the mass of explosive and on the distance to the detonation point.

To define the blast load the ABAQUS/Explicit user subroutine VDLOAD was used [25]. This subroutine allows the user to define the load as a function of position and time. The blast load was modelled as pressure acting on the exposed face of the slab. The value of the pressure is a space and time dependent function which must take into account the time taken by the overpressure peak to meet the slab, the decrease of the peak pressure value with the distance and its exponential reduction with time [28]. In order to define those aspects the following empirical expressions were used [28]:

$$
\begin{aligned}
&p(t) = 0 && t < t_{\mathrm{o}} \\
&p(t) = (p_{\mathrm{r}} - p_{\mathrm{s}})\left(1 - \frac{t - t_{\mathrm{o}}}{t - t' - t_{\mathrm{o}}}\right) + p_{\mathrm{s}}\left[1 - \frac{t - t_{\mathrm{o}}}{T_{\mathrm{s}}}\right]\exp\left\{-\frac{b(t - t_{\mathrm{o}})}{T_{\mathrm{s}}}\right\} && t_{\mathrm{o}} < t < l \\
&p(t) = p_{\mathrm{s}}\left[1 - \frac{t - t_{\mathrm{o}}}{T_{\mathrm{s}}}\right]\exp\left\{-\frac{b(t - t_{\mathrm{o}})}{T_{\mathrm{s}}}\right\} && t > t_{\mathrm{o}} + t'
\end{aligned}
\tag{7}
$$

$$
\begin{aligned}
&p_{\mathrm{s}} = \frac{1.4072}{Z} + \frac{0.5540}{Z^2} - \frac{0.0357}{Z^3} + \frac{0.000625}{Z^4}\ [\mathrm{MPa}] && 0.05 \leqslant Z \leqslant 0.3 \\
&p_{\mathrm{s}} = \frac{0.6194}{Z} - \frac{0.0326}{Z^2} + \frac{0.2132}{Z^3}\ [\mathrm{MPa}] && 0.3 \leqslant Z \leqslant 1.0 \\
&p_{\mathrm{s}} = \frac{0.0662}{Z} + \frac{0.405}{Z^2} + \frac{0.3288}{Z^3}\ [\mathrm{MPa}] && 1.0 \leqslant Z \leqslant 10
\end{aligned}
\tag{8}
$$

Table 2
Concrete mechanical properties

Density: 2400 kg/m^3
Elastic modulus: 2.5×10^4 MPa
Poisson's ratio: 0.15
Compressive elastic limit: 18 MPa
Compressive strength: 25 MPa
Internal friction angle: 30°
Dilatancy angle: 20°

Table 3
Steel mechanical properties

Density: 7800 kg/m^3
Elastic modulus: 2.1×10^5 MPa
Poisson's ratio: 0.3

Table 4
Soil mechanical properties

Density: 1200 kg/m^3
Elastic modulus: 100 MPa
Poisson's ratio: 0.3
Cohesion: 0.11 MPa
Internal friction angle: 20°

$$Z = \frac{R}{W^{1/3}}; \quad p_r = 2p_s\left(\frac{7p_o + 4p_s}{7p_o + p_s}\right),$$

$$t' = 3S/U_s; \quad U_s = \sqrt{\frac{6p_s + p_o}{7p_o}}\, a_o; \quad t_o = R/U_s, \tag{9}$$

where R is the distance to the charge, W is the mass of the explosive [kg of TNT], Z is the scaled distance, p the pressure acting on the slab, p_s is the overpressure at the wave front, p_r is the reflected pressure, p_o is the atmospheric pressure, t is the time, t_o is the time when the overpressure meets the structure, T_s is the duration of the positive overpressure phase that can be obtained from tables as a function of Z, t' is the time of incidence of the reflected pressure, b is the wave shape parameter that depends on p_s, U_s is the velocity of the wave front, a_o is sound velocity at ambient conditions, S is half the slab short side length.

Normal reflection and validity of Rankine–Hugoniot (R–H) relations were assumed. These simplifying assumptions were made in order to obtain simple analytical expressions that could be written in a user subroutine. It should be noted that these constitute great simplifications taking into account the proximity of the blast load to the slab. This fact shows one of the major drawbacks of this type of numerical analysis where the blast load has to be approximated since a complete coupled analysis cannot be performed.

To get an idea of the value of the resultant pressure magnitude and the positive phase duration, for the 12.5 kg Gelamón charge (equivalent to 10 kg TNT), for instance, the maximum resultant pressure is 110 MPa and the duration of the positive phase is around 3×10^{-4} s.

In order to define the load history, the blast loads were assumed to be applied at time intervals such that the superposition of pressure waves was negligible and the response was stabilized. The total duration of the load for the three tests was approximately 2.0×10^{-2} s.

An explicit dynamic analysis was carried out based on the central difference integration rule, which is suitable for impulsive loads and strong discontinuous responses. The central difference method is conditionally stable and the stability limit depends on the highest frequency of the

system ω_{max} [25,29]

$$\Delta t \leqslant \frac{2}{\omega_{max}}. \tag{10}$$

An approximation for this stability limit can be obtained as the shortest time interval necessary for p-waves to pass the elements of the mesh,

$$\Delta t \leqslant \min\left\{\frac{L}{c_d}\right\}, \tag{11}$$

where L is the length of the element and c_d the propagation velocity of p-waves.

ABAQUS/Explicit program [25] allows the automatic estimation of a stable time increment. With this purpose, the velocity of the dilatation wave is calculated in each element, for each time increment, assuming a hypo-elastic material model.

At first, the problem was run with automatic time increment and element by element estimation, but the response was unstable. This was due to the simplified material model employed for the estimation of the critical time increment.

In order to obtain stability, fixed time increments of 5.4×10^{-6} s were used (0.05 times the original estimation). A total of about 7.3×10^4 time increments and 90 min of CPU time were required for the simulation of the 2×10^{-2} s history.

The deformation of the slab after each of the three experiments is presented in Fig. 8. It can be seen, especially in the later tests, there is elevation of the plate corners that was also observed in experimental tests. Points A and B suffered the highest displacements which amounted to 19 and 40 mm, respectively.

Fig. 9 depicts the maximum stress distribution occurring during the first test on the upper and lower face, respectively. It is interesting to notice the traction zones in coincidence with the circumferential external cracking as revealed experimentally. Stress and strain states obtained for the lower reinforcement indicate that the yield tension was reached in correspondence to the internal circumferential crack, confirming the failure mechanism experimentally observed.
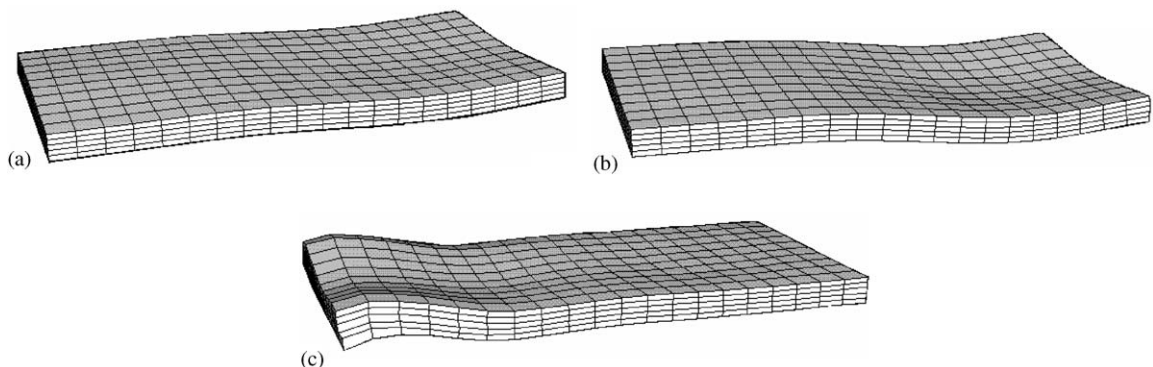

Fig. 8. Slab deformation (amplification factor: 20) (ABAQUS CAE 2-5) (a) test 1, (b) test 2, (c) test 3.

4.2. Hydrocode [26]

In contrast with the analysis done with the finite element program, the complete phenomenon was modelled in this case. New developments in integrated computer hydrocodes [30], such as the AUTODYN Software [26] used in this section, are especially suitable for the study of interaction problems involving multiple systems of structures, fluids, and gases and highly time-dependent and non-linear problems.

The analysis began with the modelling of the detonation and propagation of the pressure wave inside the explosive and in the air in contact with the explosive. As this analysis must be performed with much detail, it was done in a previous stage in which a spherical explosive was modelled with AUTODYN 2D [26,31]. Then the results of this first analysis were mapped into the three dimensional model [26]. Starting from this point, the propagation of the blast wave in air and its interaction with the plate were simulated with AUTODYN 3D.

The model was composed of the plate, the underlying soil and the air volume surrounding the plate, as shown in Fig. 10a.

A three-dimensional Euler FCT [26] (higher order Euler processor) subgrid was used for the air. Flow out of air was allowed at all the borders. To model the air a fluid with the properties presented in Table 5 was used.
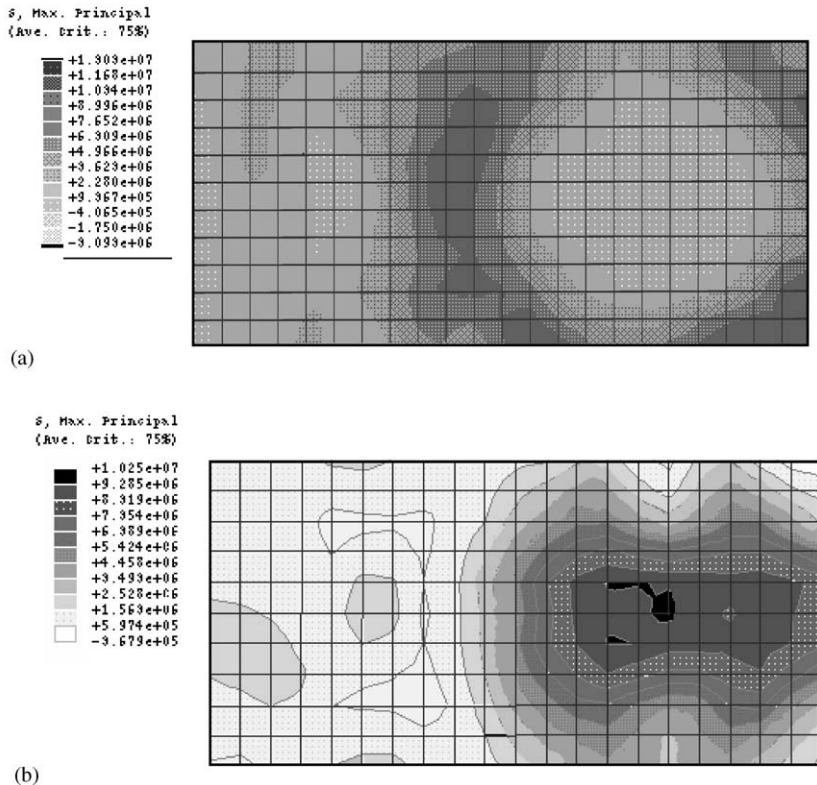

Fig. 9. Maximum stress contours (Pa) (test 1) (ABAQUS CAE 2-5)—(a) Upper face and (b) Lower face.

The reinforced concrete slab was modelled with three-dimensional solid elements that were solved with a Lagrange processor. The mesh was similar to cells that are used for the finite element analysis.

Although reinforced concrete elements can be modelled as a combination of concrete and steel elements joined together with the assumption of perfect bond, this type of model is prohibited for actual structures, as it requires a great number of elements. Moreover, the time step in explicit dynamic programs is directly related to the size of the elements. Elements which have dimensions similar to the actual reinforcement usually lead to extremely reduced time steps, making the analysis too slow.
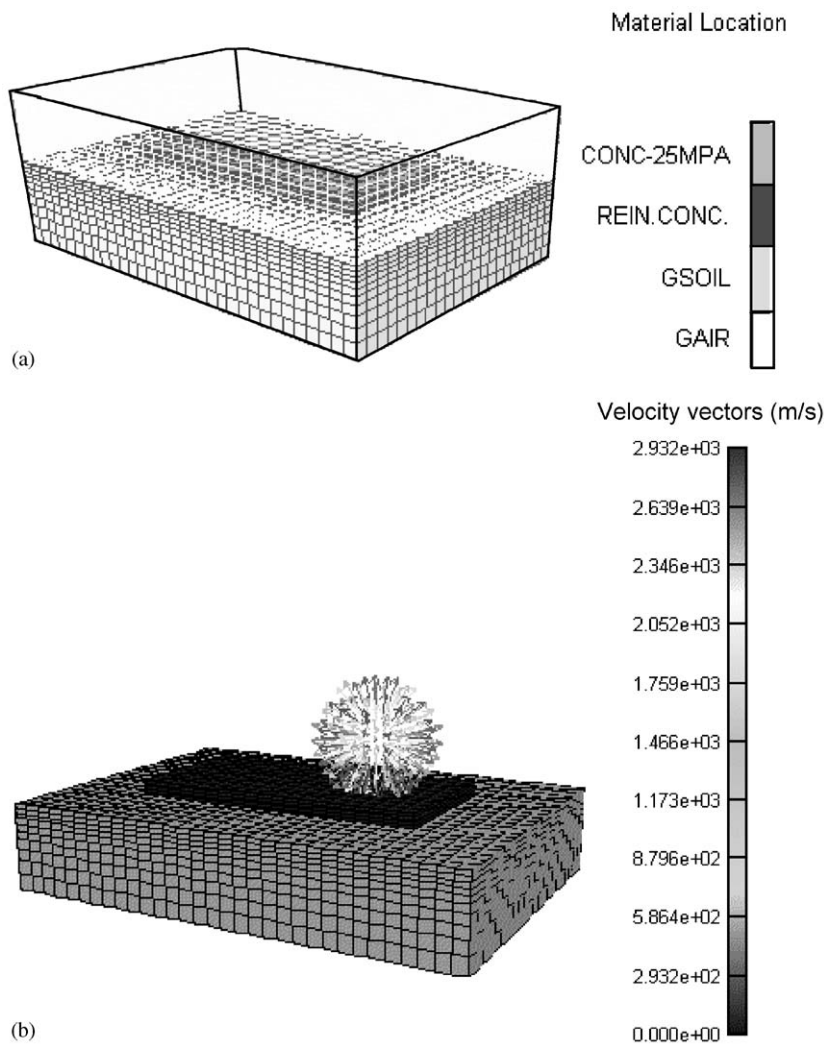

Fig. 10. Model for the simulation with AUTODYN—(a) Mesh, (b) Propagation of blast wave and interaction with the concrete plate.

Table 5
Air properties

Equation of state	Ideal gas
	$\gamma = 1.4$
	$\rho = 1.225 \times 10^{-3}\,\text{g/cm}^3$
	Ref. energy $= 0.0\,\text{mJ}$
	Press. shift $= 0.0\,\text{kPa}$
Initial conditions	$\rho = 1.225 \times 10^{-3}\,\text{g/cm}^3$
	Ref. energy $= 2.068 \times 10^5\,\text{mJ/mg}$

Table 6
Reinforced concrete mechanical properties

Density: $2400\,\text{kg/m}^3$
Elastic modulus: $2.6 \times 10^4\,\text{MPa}$
Poisson's ratio: 0.15
Compression strength: $25\,\text{MPa}$
Tension strength: $4\,\text{MPa}$

Taking into account the above considerations, an approximate material model was defined to simulate the behaviour of reinforced concrete. The model used is a homogenized elastoplastic material similar to elastoplastic models of concrete but with higher stiffness and tension strength to take into account the influence of the reinforcement. The lower layer of the plate was filled with that material while the upper layers were all filled with concrete with the same properties used for the finite element analysis. The mechanical properties of the homogenized model used for reinforced concrete are shown in Table 6.

The soil was also modelled with three-dimensional solid elements and solution was carried out with a Lagrange processor. A transmit boundary condition [26] was defined at the borders to simulate semi-infinite space. An elastoplastic model with the same mechanical properties of Table 4 was used for the soil.

Detonation is a type of reaction of the explosive that produces shock waves of great intensity. If the explosive is in contact with or near a solid material, the arrival of the shock wave at the surface of the explosive generates intensive pressure waves that can produce the crushing or the disintegration of the material. This shock effect is known as brisance [28]. Brisance produces discontinuities in the material. In order to reproduce this type of effect, the erosion model of AUTODYN [23,24,26] was used to remove from the calculation the cells that have reached certain criteria based on deformations. When a cell is eliminated, its mass is retained and concentrated at its nodes that begin to behave as free masses conserving their initial velocity.

This erosion model represents a numerical remedial measure to counteract the great distortion that can cause excessive deformation of the mesh. For this reason, its application to the simulation of a physical phenomenon requires calibration with experimental results.

The slab was simulated with different erosion models and erosion limits in order to define the appropriate erosion criteria and erosion limit. This analysis led to an erosion limit of 7.5×10^{-2} of incremental effective strain [31].

To study the structural behaviour of the plate, the propagation of the blast wave and its interaction with the plate was analysed. To do this an interaction algorithm between the Lagrange (plate) and Euler (air) processors was used [26].

As an illustration, Fig. 10b represents the velocity field in the air and pressure contours on the solids. The alteration of the blast wave produced as a result of the reflections on the plate and the ground should be noted. Because of the reflections, the blast wave increased its destructive effect in the vertical direction and lost its spherical shape.

In the analysis, the solid–solid interaction [26] between the plate and the soil was also taken into account through a contact algorithm.

The three explosions were simulated one after the other separated in time in order to assure that air pressure returned to its reference value. The total real time history simulated was about 0.03 s. Increments of time of about 1×10^{-7} were automatically defined by the program and a total of 1 h of CPU time was required.

Fig. 11 shows the results of the numerical tests. The maximum displacements registered at points A and B in this case are 28 and 66 mm that are very close to experimental measures. Fig. 11 show the crushing of concrete in the zone of the slab directly beneath the charge. The deformed shape obtained is in accordance with the failure mechanism assumed in limit analysis where the effect of the underlying soil was supposed to be negligible.

5. Conclusions

Based on experimental results, an equation that approximately relates the crater diameter on the pavement with the explosive charge and its height above the pavement was proposed.

Due to the relatively low strength and stiffness of the underlying soil, the presence of soil does not alter the plate behaviour. The failure shape is almost coincident with that of a circular simply-supported plate and with the diameter equal to the short side of the slab. The deformed shape of the plate can be approximately depicted by a truncated cone.

For this case, limit analysis seems to be a simple and valuable tool to estimate the effect of a blast load or to determine the magnitude of the explosive charge when the damage has already been done. Eq. (6) can be used to estimate the pressure producing the damage observed and then, with the aid of Eqs. (8) and (9) or charts that can be found in blast references [28], the charge producing that crater can be estimated.

Both the finite element program and the hydrocode used approximately reproduce the deformation and the resultant failure shape of the plate under the blast load. In both cases an explicit dynamic analysis was required with very small time increments and a high computational cost. Nevertheless, hydrocodes seems to be more appropriate for the simulation of the complete interaction problem with less computational effort.

Although the constitutive models used in the analysis were quite simple, they were able to describe a similar response to the one observed experimentally. An important limitation is, however, the modelling of the discrete cracking which cannot be done with the model employed.
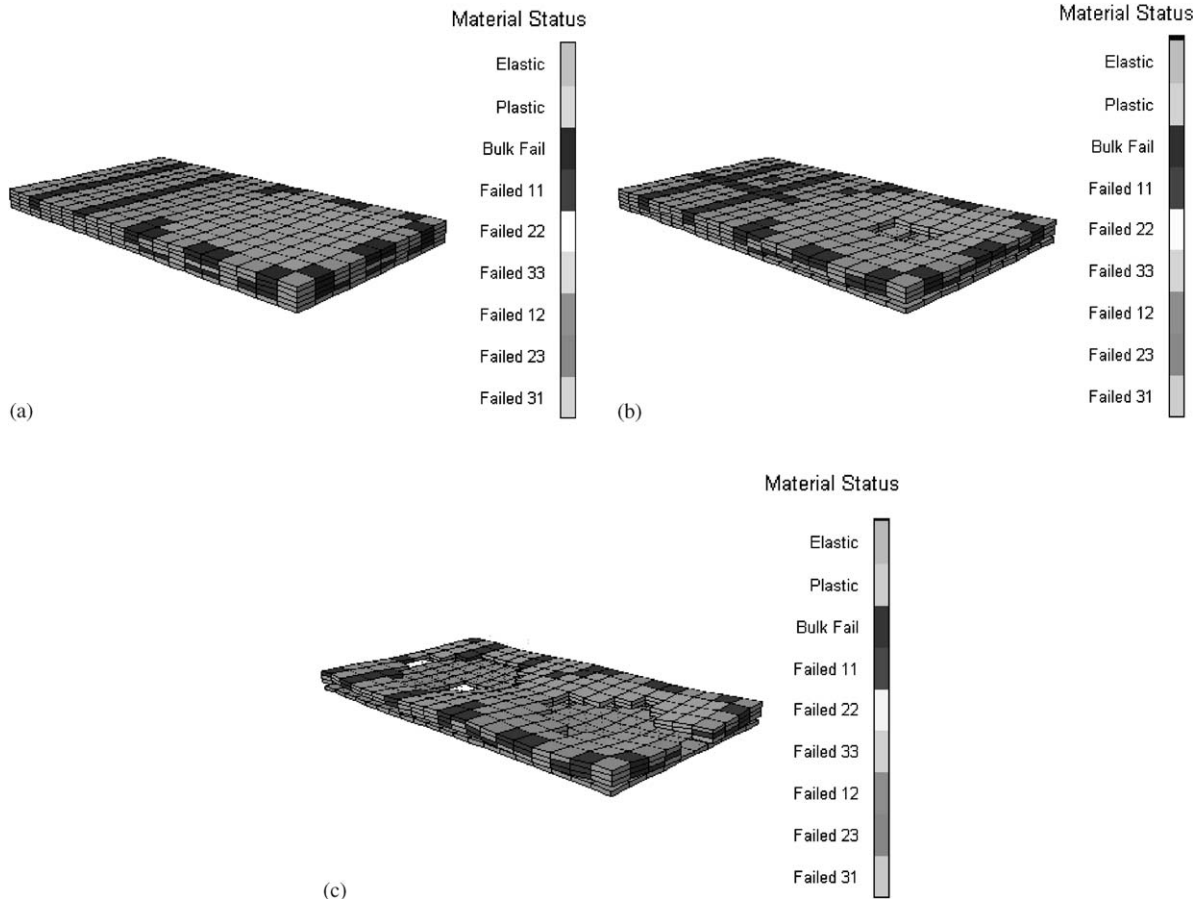
Fig. 11. Deformed shape (magnification factor: 2) and concrete crushing. (a) test 1, (b) test 2, (c) test 3.

In particular, it was not possible to reproduce the division of the plate in two parts. As a result, the maximum vertical displacement obtained with the finite element model was significantly lower than the one measured experimentally for the third explosion using a 12.5 kg charge.

More experimental data related to craters produced by explosive loads above concrete pavements is needed. Some research effort must still be done in order to define a more suitable erosion model for concrete. Erosion models for concrete must be based on damage and failure criteria that take into account the different response in compression and tension.

Acknowledgements

References

[1] Elliot CL, Mays GC, Smith PD. The protection of buildings against terrorism and disorder. Proc Inst Civil Eng: Struct Build 1992;94:287–97.

[2] Elliot CL, Mays GC, Smith PD. The protection of buildings against terrorism and disorder. Discussion. Proc Inst Civil Eng: Struct Build 1994;104:343–50.

[3] Committee on Feasibility of Applying Blast-Mitigating Technologies and Design Methodologies from Military Facilities to Civilian Buildings. Protecting buildings from bomb damage. Washington: National Academy Press; 1995.

[4] Malvar LJ, Crawford JE, Wesevich JW, Simons D. A plasticity concrete material model for DYNA3D. Int J Impact Eng 1997;(9–10):847–73.

[5] Comi C, Perego U. On visco-damage models for concrete at high strain rates. Computational plasticity, fundamentals and applications. Barcelona: CIMNE; 1997.

[6] Dubé JF, Pijudier-Cabot G. Rate-dependent damage model for concrete in dynamics. J Eng Mech ASCE 1996;122(10):939–47.

[7] Sercombe JF, Ulm J. Viscous hardening plasticity for concrete in high rate dynamics. Computational Plasticity, Fundamentals and Applications. Barcelona: CIMNE; 1997.

[8] Sercombe J, Ulm F, Toutlemonde J. Viscous hardening plasticity for concrete in high rate dynamics. J Eng Mech ASCE 1998;124(9):1050–7.

[9] Luege M, Luccioni B, Danesi R. Modelo de Daño Dependiente de la Velocidad de Deformación. Rev Int Métodos Numéricos para Cálculo y Diseño en Ingeniería 2002;18(2):411–31.

[10] Jacinto A, Ambrosini RD, Danesi RF. Experimental and computational analysis of plates under air blast loading. Int J Impact Eng 2001;25(10):927–47.

[11] Jacinto A, Ambrosini RD, Danesi RF. Dynamic response of plates subjected to blast loading. Proc Inst Civil Eng: Struct Build 2002;SB152(3):269–73.

[12] Yi P. Explosionseinwirkungen auf Stahlbetonplatten. Zur Erlangung des akademischen Grades eines Doktor-Ingenieurs der Fakultät für Bauingenieur- und Vermessungswessen der Universität Fridericiana zu Karlsruhe (TH), 1991.

[13] Mays GC, Hetherington JG, Rose TA. Response to blast loading of concrete wall panels with openings. ASCE J Struct Eng 1999;125(12):1448–50.

[14] Lok TS, Xiao JR. Steel-fibre-reinforced concrete panels exposed to air blast loading. Proc Inst Civil Eng Struct Build 1999;134:319–31.

[15] Lubliner J. Plasticity theory. USA: McMillan; 1990.

[16] Toutlemonde F, Rossi P. Major parameters governing concrete dynamic behaviour and dynamic failure of concrete structures. DYMAT J 1995;2(1):69–77.

[17] Brara A, Camborde F, Klepaczko JR, Mariotti C. Experimental and numerical study of concrete at high strain rates in tension. Mech Mater 2001;33:33–45.

[18] Le Nard H, Bailly P. Dynamic behaviour of concrete: the structural effects on compressive strength increase. Mech Cohes-Frict Mater 2000;5:491–510.

[19] Cadoni E, Labibes K, Berra M, Giangrasso M, Albertini C. High-strain-rate tensile behaviour of concrete. Mag Concrete Res 2000;52(5):365–70.

[20] López Cela JJ. Analysis of reinforced concrete structures subjected to dynamic loads with a viscoplastic Drucker–Prager model. Appl Math Modelling 1998:495–515.

[21] Zheng S, Haussler-Combe U, Eibl J. New approach to strain rate sensitivity of concrete in compression. ASCE J Eng Mech 1999;125(12):1403–10.

[22] Eibl J, Schmidt-Hurtienne B. Strain-rate-sensitive constitutive law for concrete. ASCE J Eng Mech 1999;125(12):1411–20.

[23] Gebbeken N, Ruppert M. A new material model for concrete in high-dynamic hydrocode simulations. Arch Appl Mech 2000;70:463–78.

[24] Gatuingt F, Pijaudier-Cabot G. Computational modelling of concrete structures subjected to explosion and perforation. In: Proceeding of Eccomass 2000, Barcelona, 2000.

[25] ABAQUS/Explicit User's Manual, Version 6.1, V I & II, Hibbitt, Karlsson & Sorensen, Inc., 2000.
[26] AUTODYN. Interactive Non-Linear Dynamic Analysis Software, Version 4.2, User's Manual. Century Dynamics Inc., 2001.
[27] Ambrosini D, Luccioni B, Danesi R, Riera J, Rocha M. Size of craters produced by explosive charges on or above the ground surface. Shock Waves 2002;2(1):69–78.
[28] Smith PD, Hetherington JG. Blast and ballistic loading of structures. Oxford, UK: Butterworth Heinemann Ltd; 1994.
[29] Bathe KJ. Finite element procedures in engineering analysis. Englewoods Cliffs, NJ: Prentice-Hall; 1982.
[30] Mair HU. Review: hydrocodes for structural reponse to underwater explosions. Shock and Vibration 1999;6:81–96.
[31] Luccioni B, Ambrosini D, Danesi R. Analysis of building collapse under blast loads. Eng Struct 2004;26:63–71.